Petroleum and Coal

Article **Open Access**

CFD SIMULATION AND EXPERIMENTAL STUDY ON CO_2 CAPTURE IN FLUIDIZED BED REACTOR USING DRY POTASSIUM-BASED SORBENT

Mahdi Ayobi[1], Shahrokh Shahhosseini[1], Yaghoub Behjat[2]

[1] *School of Chemical Engineering, Iran University of Science and Technology, Tehran, Iran*
[2] *Process Development and Equipment Technology Division, Research Institute of Petroleum Industry, Tehran, Iran*

Received May 13, 2019; Accepted July 31, 2019

Abstract

The process of CO_2 capturing using solid sorbents is highly cost-effective and energy efficient. In this research, experimental and computational studies of CO_2 sorption from a flue gas stream using potassium carbonate particles have been conducted, employing a laboratory scale bubbling gas solid fluidized bed reactor. The influences of the main operating conditions such as CO_2 and H_2O concentrations and gas mixture velocity on the CO_2 removal have been investigated. An Eulerian–Eulerian two-fluid approach based upon the kinetic theory of granular flow with modified energy-minimization multi-scale (EMMS) interphase exchange coefficient was applied to describe the gas–solid hydrodynamic in the fluidized bed. The computational model results of the slug rise velocity, bubbles, and solid phase behavior and CO_2 concentration along the fluidized bed height have been compared with corresponding experimental data. The CFD simulation results are in good agreement with the measured experimental data. Both simulation results and experimental measurements of the outlet CO_2 concentration show that good treatment efficiency can be obtained by maintaining H_2O concentration as the maximum value. The CO_2 removal rate increased due to the reduction of gas velocity as well as increasing H_2O concentration. Among the factors studied, H_2O concentration has the most significant impact on the CO_2 adsorption.

Keywords: *CO_2 capture; CFD; Gas –solid; Fluidized bed; Adsorption; Simulation.*

1. Introduction

Recent researches suggest that greenhouse gas emissions (GHG) should be reduced in order to avoid intense climate changes. The primary greenhouse gas, which is mainly released by burning fossil fuels, is carbon dioxide (CO_2) [1-2]. There are some approaches to decrease the net CO_2 emissions into the atmosphere, including reduction of energy consumption by improving the efficiency of energy conversion, switching to less carbon intense fuels, and using alternative energies [3]. However, it is understood from the project of Energy Information Agency (EIA) of U.S.A. that for the foreseeable future, coal will continue to play an important role in electricity generation, especially in some powerhouse plants [4]. Therefore, these approaches may not be enough to achieve a desirable atmospheric CO_2 concentration in the near future. Nowadays, absorption and storage of CO_2 seem to be a very important approach. There are some techniques that can be used to separate CO_2 from a flue gas stream such as wet absorption, adsorption, membrane separation, and cryogenic separation. However, these methods face the limitations of cost and energy required to treat the massive flue gas streams from fossil fuel powerhouse plants [5-7].

Recently, CO_2 chemical adsorption by the use of recoverable solid adsorbents has been studied as an alternative method. Applying the solid adsorbents have some advantages over other types, including the high capacity for chemical adsorption, low thermal capacity, and possible production of pure carbon dioxide. The solid sorbents capture CO_2 from flue gases through chemical adsorption, physical adsorption, or a combination of them [8-9].

A number of researchers have used chemical sorbents due to high adsorption capacity and selectivity of them to adsorb carbon dioxide in comparison with physical sorbents. It is reported that potassium carbonate shows the best performance in comparison with other alkali based chemical sorbents [9-10].

Anhydrous potassium carbonate solid particles react with CO_2 and existing moisture in the gas flow of the fluidized bed system to yield potassium bicarbonate as follows:

$$K_2CO_3(s) + CO_2(g) + H_2O(g) \longleftrightarrow 2KHCO_3(s) \quad (1)$$

Several types of research have also been performed aiming at the applications of this sorbent for industrial purposes. Some researchers have conducted great efforts to coat various supports by K-based sorbents and find out the reaction characteristics of the potassium based solid sorbent [1,11-13]. However, the effects of the operating conditions on the carbonation reactions were not completely identified.

Zhao *et al.* [14] studied the effects of the reaction conditions on the carbonation characteristics of K_2CO_3 calcinated from $KHCO_3$ with a pressurized thermos gravimetric apparatus. Their results show that the conversion rate decreases as the reaction temperature and pressure increases, and the effects of CO_2 and H_2O concentrations are little compared to other factors [14].

Zhao *et al.* [15] have investigated the carbonation behaviors of K_2CO_3/Al_2O_3 using thermos gravimetric analyzer in a bubbling fluidized bed. They supposed that the main carbonation product of K_2CO_3/Al_2O_3 is $KHCO_3$ and so the effects of the temperature, gas composition, and pressure on the reactions were studied by analyzing the adsorbent weight change. Their result shows that the total carbonation conversion increases with the increase of CO_2 and H_2O concentrations but decreases with the increase of the temperature and pressure [15].

Yi *et al.* [16] have surveyed the CO_2 capture process using potassium carbonate-based solid sorbent (Sorb KX35) in the continuous solid circulation mode between two fluidized bed reactors, detecting CO_2 concentration in the carbonation reactor exhaust. They have reported that the CO_2 removal escalates as gas velocity decreases and as solid circulation rate increases. Increasing the solid circulation rate or the water vapor content and decreasing the gas velocity raises the overall CO_2 removal in this system [16].

In the solid sorbent process, heat transfer rate control is necessary to prevent the formation of hot spots during highly exothermic adsorption reactions. Fluidized bed reactors can be the best choice for CO_2 capture by solid adsorbent due to their high efficiency of heat and mass transfer owing to the greater contact surface between the gas and solid particles. Meanwhile, they prevent the formation of hot zones by creating almost isothermal conditions due to the quick circulation of the particles in the reactor. Therefore, many researchers have utilized fluidized bed reactors instead of fixed bed reactors for the adsorption process.

Mathematical modeling is an important tool to investigate the performance of the adsorption process in terms of identifying effective parameters and predicting adsorption behavior in the reactor. Application of computational fluid dynamic (CFD) simulation is known as a technique to predict fluid dynamics and transport phenomena of the multiphase flows, especially where the prediction of the flow behavior is rather difficult and expensive through experimental techniques. Development of multidimensional models for hydrodynamics, heat transfer, and chemical reactions of complicated gas-solid processes have recently attracted considerable attentions. The required time for CFD modeling has been decreased by improvements in numerical methods and hardware technological advancements. Thus, once the model has been validated, CFD can be utilized for sensitivity analysis due to its flexibility in changing the parameters [17-18].

Numerous researchers have studied the hydrodynamics of the gas-solid fluidized bed employing CFD techniques, although CFD simulation of CO_2 capture process in the fluidized bed is not much emphasized.

Khongprom and Gidaspow [19] simulated the CO_2 capture process by potassium carbonate in two dimensional circulating fluidized bed reactor using the kinetic theory of granular model. They compared computed total granular temperatures in different gas velocity with the literature values. Their CFD simulation results show that 90% of CO_2 removal can be achieved by adjusting the bed height and gas velocities [19].

Garg *et al.* [20] performed CFD simulation of CO_2 capture using dry potassium based sorbent applying the open-source CFD solver MFIX. They compared their simulation results with continuous CO_2 capture experimental data and found that the sensitivity of CO_2 removal with respect to the solid mass flow rate was within 2% of the experimental sensitivity [20].

Chalermsinsuwan *et al.* [21] applied the CFD simulation of the circulating fluidized bed sorption-regeneration system for removal of CO_2 from flue gases by K_2CO_3 solid sorbent. They found that the reactor length, solid sorbent density and diameter had less effect on the CO_2 removal than the inlet gas velocity and reaction rate constant indicating the effects of operating conditions, including the gas composition and gas flow rate on the carbonation reactions are essential for describing the carbonation behaviors and determining appropriate reaction conditions of this sorbent [21].

For better understanding the hydrodynamic characteristics and CO_2 adsorption process behavior in a bubbling gas-solid fluidized bed reactor, a lab-scale fluidized bed has been built to capture CO_2. The measured experimental data has been used to better understand the hydrodynamic and CO_2 adsorption phenomena, as well as validating the developed computational model. The computational fluid dynamics (CFD) model has been employed using Eulerian-Eulerian approach with a modified drag model that is proposed using a scaling factor to reduce the universal drag laws, which accounts for the effect of particle clustering. In this research, the effects of CO_2 and H_2O concentrations and superficial gas velocity on CO_2 adsorption rate have been investigated both experimentally and in a CFD simulation environment.

2. Experimental setup and methods

Several tests have been conducted to investigate carbon dioxide adsorption process and hydrodynamics of the gas-solid flow in the fluidized bed. Additionally, the data acquired using the experimental setup have been applied to evaluate the developed computational model. Figure 1 depicts a schematic picture of the fluidized bed experimental setup, which is comprised of three main parts: a gas injection system, a carbon dioxide gas adsorption system and a CO_2 analyzer. The fluidized bed reactor was a column, made of Plexiglas, with 0.063 m diameter and 1 m height. The 0.453 kg of the solid adsorbent was placed in the reactor, which occupies some 0.1 m of the bed height. The size distribution of the spherical adsorbent particles was within 200-800 μm with a mean size of 600 μm and density of 2300 kg/m^3.

The mixture of water and carbon dioxide was injected at the bottom of the bed through a perforated plate (gas distributor). The CO_2 content of the inlet gas flow was adsorbed by a K_2CO_3 solid adsorbent in the bed, while the moisture required for the reaction was supplied by an auxiliary steam boiler. Gas flow rate, humidity, and carbon dioxide contents of the air were measured by the flow meters installed inside of the flow path.

The concentration of carbon dioxide of the outlet gas flow was measured using a standard gas analyzer (Testo 327), mounted at the end of the bed. Taking into consideration the operation temperature (60-70°C), a heating system was used to heat up the mixture flow of the air and carbon dioxide. The hydrodynamic structure of the gas-solid flow was characterized using high-intensity uniform illumination by installing two sources of distributed light behind the bed and using a commercial digital camera (Casio EX-F1) with the photography rate of 1200 frame per second. A black sheet was used to cover all around the bed to shield the light in order to avoid any shading and direct reflections of the surrounding environment on the walls of the bed. Bubble formation in the bed created some transparent areas, which could pass through the emitted lights and let them reach the lens of the camera. Thereby, one could observe and trace the bubbles.

In order to study the effects of carbonation reaction conditions, carbonation of K_2CO_3 was carried out under a wide range of reaction conditions. In the simulation, concentrations of CO_2 and H_2O at the inlet flue gas were chosen to be between 10 % and 20 % and inlet gas mixture velocity was in the range 0.71 to 1.1 m/s. The behavior of the CO_2 capture process was evaluated by determining the CO_2 concentration of the outlet flow. The baseline operating conditions at the inlet of the fluidized-bed carbonator are 60^{0}C carbonator temperature, 0.71 m/s gas velocity, and 15% the mixture of water vapor and carbon dioxide.

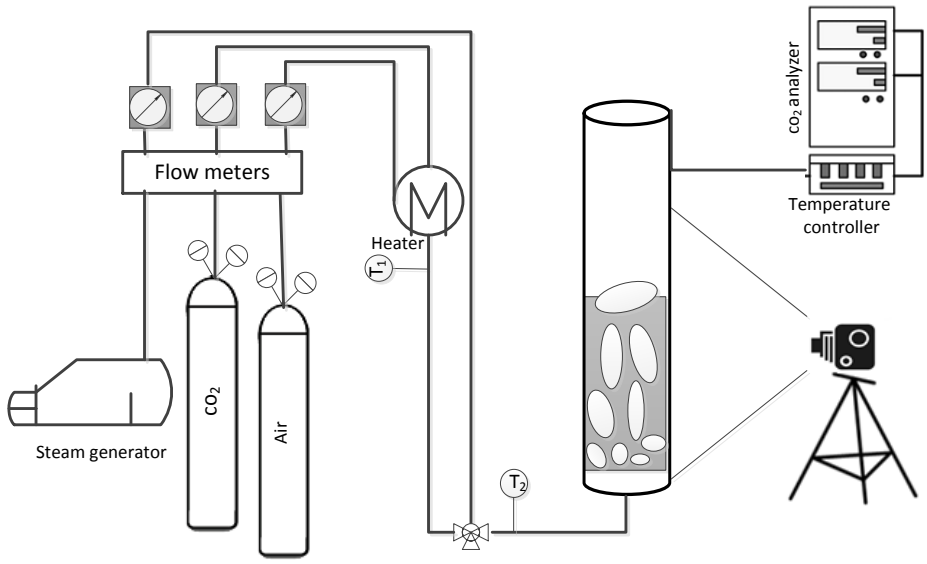

Figure 1. A schematic picture of the experimental set up

3. Model description and governing equations

A computational model of the adsorption process in the bubbling gas solid fluidized bed reactor includes bed hydrodynamics and CO_2 adsorption kinetics. In this model, conservation equations of mass, momentum, and species were formulated for gas and solid phases using the Eulerian approach, which considers both gas and solid as interpenetrating continua. The governing equations were then closed by using constitutive equations based on the kinetic theory of granular flow. The source terms were appeared in momentum and continuity equation due to the heterogeneous reactions between two phases. The reaction rate part of the species conservation equation expresses the production and consumption rates of these species. The conservation and constitutive equations for each phase are provided as below:

3.1. Conservation equations

The developed computational model includes continuity, momentum, and chemical species conservation equations are considered based upon the assumption that the system is isothermal. Under this assumption, energy conservation can be ignored. The continuity equation for gas and solid phases is stated by the following equations:

$$\frac{\partial}{\partial t}\left(\varepsilon_g \rho_g\right) + \nabla.\left(\varepsilon_g \rho_g u_g\right) = S_{gs} \quad (2)$$

$$\frac{\partial}{\partial t}\left(\varepsilon_s \rho_s\right) + \nabla.\left(\varepsilon_s \rho_s u_s\right) = S_{sg} \quad (3)$$

Taking into account, the heterogeneous reaction between the gas and solid phases (CO_2 adsorption), the term (S) is used to express the interphase mass transfer in the continuity equation, which is defined as follows.

$$S_{gs} = -R\left(M_{CO_2} + M_{H_2O}\right) \quad (4)$$

Equation (4) can be applied to calculate momentum for the gas phase.

$$\frac{\partial}{\partial t}\left(\varepsilon_g \rho_g u_g\right) + \nabla.\left(\varepsilon_g \rho_g u_g u_g\right) = \varepsilon_g \rho_g g - \varepsilon_g \nabla P \quad + \nabla \varepsilon_g \tau_g + \beta_{gs}\left(u_s - u_g\right) + S_{gs} u_g \quad (5)$$

where β_{gs} is the drag coefficient between the gas and solid phases. At the right side, $S_{gs}u_g$ indicates the momentum transfer in the gas phase as a result of mass transfer. The momentum equation of the solid phase is presented by the following equation,

$$\frac{\partial}{\partial t}(\varepsilon_s\rho_s u_s)+\nabla.(\varepsilon_s\rho_s u_s u_g)=\varepsilon_g\rho_g g-\varepsilon_g\nabla P\quad+\nabla\varepsilon_s\tau_s-\beta_{gs}(u_s-u_g)+S_{sg}u_s \tag{6}$$

Considering CO_2 adsorption by solid particles, the mass transfer occurs between a solid phase and the gas phase. Therefore, individual species conservation equation for CO_2 and steam in the gas phase was written as follows:

$$\frac{\partial}{\partial t}(\varepsilon_j\rho_j Y_{j,i})+\nabla.(\varepsilon_j\rho_j Y_{j,i}u_j)=-\nabla\varepsilon_j J_{j,i}+R_{s,i} \tag{7}$$

While $J_{g,i}$ and $R_{s,i}$ denote diffusion flux of component i and rate of heterogeneous reaction, respectively. The fluctuating kinetic energy conservation equation for the solids modeled from the concept of the kinetic theory of gases for inelastic nature of the particles collisions, be expressed as:

$$\frac{3}{2}\frac{\partial}{\partial t}(\varepsilon_s\rho_s\theta_s)+\frac{3}{2}\nabla.(\varepsilon_s\rho_s\theta_s u_s)=\left[(-p_s I+\tau_S):\nabla u_s+\nabla.(k_\theta\nabla\theta)-\gamma+\varphi_{gs}\right] \tag{8}$$

The terms on the right side indicate the rate of granular energy generation due to shear, diffusion transfer of granular temperature, and the losses due to inelastic collisions and friction of the fluid.

3.2. Constitutive equations

Constitutive equations are required to complete the governing equations of gas-solid flow. The following are the required constitutive equations. The stress tensor of gas-phase:

$$\tau_{g,ij}=\mu_g\left(\frac{\partial u_{g,j}}{\partial x_i}+\frac{\partial u_{g,i}}{\partial x_j}\right) \tag{9}$$

The solid-phase stress tensor:

$$\tau_{s,ij}=\mu_s\left(\frac{\partial u_{s,j}}{\partial x_i}+\frac{\partial u_{s,i}}{\partial x_j}\right)+\left(\zeta_s-\frac{2}{3}\mu_p\right)\frac{\partial u_{s,k}}{\partial x_k}\delta_{i,j}-p_s\delta_{i,j} \tag{10}$$

Granular-phase shear viscosity is composed of three terms: collisional (particle-particle collisions), kinetic (fluctuating motion) and frictional viscosity, as suggested by Syamlal *et al.* [22].

$$\mu_s=\frac{4}{5}\varepsilon_s\rho_s d_s(1+e)g_0\left(\frac{\theta_s}{\pi}\right)^{\frac{1}{2}}+\frac{d_s\rho_s\varepsilon_s\sqrt{\theta_s\pi}}{6(3-e_{ss})}\left[1+\frac{2}{5}(1+e_{ss})(3e_{ss}-1)\varepsilon_s g_0\right]+\frac{p_s\sin\phi}{2\sqrt{I_{2D}}} \tag{11}$$

The solid bulk viscosity accounts for the resistance of the solids to compression and expansion:

$$\xi_s=\frac{4}{5}\varepsilon^2{}_s\rho_s d_s(1+e)g_0\left(\frac{\theta_s}{\pi}\right)^{\frac{1}{2}} \tag{12}$$

The radial distribution function is a correction factor in calculating the probability of the collisions between the particles:

$$g_0=\frac{3}{5}\left[1-\left(\frac{\varepsilon_s}{\varepsilon_{s,\max}}\right)^{\frac{1}{3}}\right]^{-1} \tag{13}$$

The particle pressure composed of kinetic and collisional terms is calculated as follows:

$$p_s=\varepsilon_s\rho_s\theta_s+2(1+e)\varepsilon_s^2 g_0\rho_s\theta_s \tag{14}$$

The diffusion coefficient for the solid phase energy fluctuation is:

$$k_{\theta s}=\frac{15d_s\rho_s\varepsilon_s\sqrt{\theta_s\pi}}{4(41-33\eta)}\left[1+\frac{12}{5}\eta^2(4\eta-3)\varepsilon_s g_0+\frac{16}{15\pi}(41-33\eta)\eta\varepsilon_s g_0\right];\ \eta=\frac{1}{2}(1+e_{ss}) \tag{15}$$

The dissipation of fluctuating energy due to inelastic collisions takes the following form:

$$\gamma=3(1-e^2)\varepsilon_s^2 g_0\rho_s\theta_s d_s\left[\frac{4}{d_s}\left(\sqrt{\frac{\theta_s}{\pi}}\right)-\nabla u_s\right] \tag{16}$$

3.3. Drag laws and chemical reaction model of the gas adsorption process

The momentum transfer between gas and solid phases are taken into account using the drag coefficient. Wachem *et al.* demonstrated that the simulation results were highly sensitive

to the model of interphase exchange coefficient in comparison with other parameters [23]. Therefore, proper selection of the drag model is necessary for a successful simulation of the fluidized bed hydrodynamics. McKeen and Pugsley [24] beside Taghipour *et al.* [25] have reported that their relatively poor simulation results are probably due to the removal of significant forces between the particles. Existence of an adhesive force between the particles leads to agglomeration and clustering of them, which can increase particle diameter and decrease interphase exchange coefficient as well. Several drag models are developed based on the homogenous distribution of the solid particles, which are not usually observed in the operational systems. An unmodified interphase exchange coefficient is thus unable to consider the cluster formation phenomenon and causes a severe over-estimation of the bed expansion. Several modifications have been made on standard drag equations. For example, McKeen and Pugsley [24] and Arastoopour and Gidaspow [26] have used the effective size of the cluster to improve prediction of the simulations. Seu-Kim and Arastoopour have modified the kinetic theory of granular flow by developing a model of complicated additional forces [27]. Wang et al., have suggested a model, which is able to predict a correct bed expansion without further modifications. However, their proposed method was inappropriate for large-scale fluidized bed systems [28]. Recently, several researchers have utilized EMMS model to calculate the gas-solid force in heterogeneous conditions. In this study, EMMS interphase exchange coefficient, pioneered by Yang *et al.* [29] was applied and developed as follows:

$$\beta_{gs} = 150\frac{(1-\varepsilon)^2\mu_g}{\varepsilon_g {d_p}^2} + 1.75\frac{(1-\varepsilon)\rho \quad |u_g - u_s|}{d_p} \qquad \varepsilon_g \le 0.74 \tag{17}$$

$$\beta_{gs} = \frac{3}{4}\frac{(1-\varepsilon)\varepsilon_g}{d_p}\rho_g|u_g - u_s|C_{D0}H(\varepsilon_g, Re) \qquad \varepsilon_g \le 0.74 \tag{18}$$

$$C_{D0} = \frac{24}{Re(1+0.15Re^{0.687})}\ Re \le 1000; \quad C_{D0} = 0.44 \quad Re \ge 1000; \qquad Re = \frac{\rho_g \varepsilon_g |u_g - u_s| d_p}{\mu_g} \tag{19}$$

H_d is the heterogeneous factor or correction coefficient that is defined as the ratio of the drag coefficient calculated from EMMS model to standard drag coefficient. The following equation was used to express the heterogeneous factor.

$$\begin{aligned} &H\left((\varepsilon_g, Re)\frac{0.0214}{4(\varepsilon_g - 0.7463)^2 + 0.0044}{}_g\right); && 0.74 \le \varepsilon_g \le 0.82 \\ &H\left((\varepsilon_g, Re)\frac{0.0038}{4(\varepsilon_g - 0.7789)^2 + 0.004}{}_g\right); && 0.82 \le \varepsilon_g \le 0.97 \\ &H(\varepsilon_g, Re) = -31.8295 + 32.8295\varepsilon_g && \varepsilon_g \ge 0.97 \end{aligned} \tag{20}$$

3.4. Chemical reaction model of the gas adsorption process

The carbonation reaction (equation (1)) is a non-catalytic heterogeneous gas-solid reaction. There is not sufficient information about the rate equation in the literature, and most of the researches have just concentrated on preparation and adsorption characteristics of the adsorbents.

Sharonov *et al.* [30] have presented kinetics of CO_2 absorption using K_2CO_3 adsorbent. They have reported the adsorption rate to be first order with respect to CO_2 concentration ignoring the effect of moisture content on the rate equation. Park *et al.* [31] measured output concentration of CO_2 in a fixed bed in order to determine the kinetics of carbon dioxide absorption reaction in the presence of moisture by potassium carbonate. They finally concluded that the deactivation model for the non-catalytic heterogeneous reaction of CO_2, K_2CO_3, and moisture was in agreement with the corresponding experimental data. Due to the higher concentration of steam at the inlet than carbon dioxide, its concentration was assumed to be constant [31]. Kinetic equations used by various researchers for simulation of CO_2 adsorption process in fluidized bed reactor have been summarized in Table 1.

Table 1. Proposed kinetic equations used by various researchers

Khongprom and Gidaspow [19]	$r = -k_{reaction} C_{CO_2} C_{H_2O} \varepsilon_s$	(21)
Garg *et al.* [20]	$r = -k_{reaction} C_{CO_2} C_{K_2CO_3} \varepsilon_s$	(22)
Chalermsinsuwan *et al.* [21]	$r = -k_{reaction} C_{co_2} \varepsilon_s$	(23)

H_2O content seems to be an effective parameter on the kinetics of the reaction considering water vapor content in conventional flows of flue gases (10-15%) and the increased conversion by raising H_2O content at the inlet [15]. Thus, in this research, the following kinetic equation was proposed and used to model the chemical reaction:

$$r = -k_{reaction} C_{CO_2} C_{H_2O} \varepsilon_s \quad (24)$$

3.5. Boundary and initial conditions

In each experiment, the reactor was filled with K_2CO_3 adsorbent with a porosity of 0.63% and up to the height of 0.1 m. Corresponding gas flow velocity and composition were specified at the fluidized bed inlet. At the outlet boundary, the flow was assumed to be fully developed. The boundary conditions for the gas phase velocity were assumed to be a no-slip condition on the walls. Johnson and Jackson boundary conditions were used as below for tangential velocity of the solid phase velocity and granular temperature on the walls [32]:

$$u_{s,w} = -\frac{6\mu_s \varepsilon_{s,max}}{\pi \phi \rho_s \varepsilon_s g_0 \sqrt{3\theta}} \frac{\partial u_{s,w}}{\partial n} \quad (25)$$

$$\theta_w = -\frac{k_s \theta}{\gamma_w} \frac{\partial \theta_w}{\partial n} + \frac{\sqrt{3}\pi \phi \rho_s \varepsilon_s u_s^2 g_0 \theta^{\frac{3}{2}}}{6\varepsilon w_{s,max}}; \ \gamma_w = \frac{\sqrt{3}\pi (1 - e_w^2) \rho_s \varepsilon_s g_0 \theta^{\frac{3}{2}}}{4\varepsilon_{s,max}} \quad (26)$$

4. Results and discussion

The governing equations were solved using the finite volume method, while the second order upwind schemes were used for discretization. Phase coupled SIMPLE algorithm, which is developed from SIMPLE algorithm for multiphase flow, was used to solve the pressure-velocity coupled equations. Furthermore, mesh sensitivity study has been done to select the number of cells, which provides numerical results independent on the meshing [33]. The simulations have been conducted using a parallel processing system (8 cores @ 3.4 GHz) due to the long computational time of CFD simulations.

In the first part of this section, simulation results of gas-solid fluidized bed hydrodynamics, including slug rise velocity, the coalescence of bubble and solid flow structure, are compared with the experimental results and corresponding data of the literature. In the next part, the carbonation reaction behavior at different inlet gas concentrations of CO_2 and H_2O and gas mixture velocities are investigated experimentally and computationally.

4.1. Hydrodynamic modeling of the fluidized bed reactor

As mentioned in the section of governing equations, the values of the bed expansion, computed using homogenous drag models, usually disagree those of experimental work. Therefore, an experimental analysis is performed to specify solid phase bed expansion ratio in the bed for various superficial velocities of the gas.

So far, no particular method has been proposed to define parameter (C) in equation (10) regarding the dependency of scale parameter to experimental conditions. Grace and Sun [34] as well as Chalermsinsuwan *et al.* [35] have reported that using the above mentioned drag model alone cannot satisfy the experimental results. That is why they have introduced a new parameter (C) into the drag model that provides reasonable results for the bed expansion. The newly introduced parameter (C) represents the effects of changing operational conditions and gas-solid properties on the drag model as follows:

$$\beta_{gs,new} = C \beta_{gs} \quad (27)$$

In this work, CFD simulations were implemented using scale parameters of 0.1, 0.2, 0.15, 0.3, 0.5 and 1, which are compared with the experimental results in terms of bed expansion in order to determine correct values of the scale factor for the modified EMMS interphase exchange coefficient.

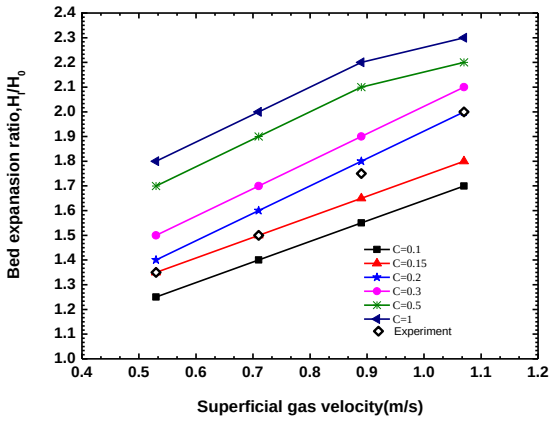

Figure 2. Bed expansion ratio for the modified EMMS interphase exchange coefficient model with different scale factors

The bed expansion ratio simulation results are compared with those of experimental data in Figure 2. General trends of the simulation results indicate a uniform increase of the bed expansion ratio with raising gas velocities. The most consistent scale factor with the experimental results is 0.15 for superficial gas velocities of 0.53 and 0.71 m/s and the scale factor of 0.2 for superficial gas velocities of 0.89 and 1.1 m/s. Therefore, the scale factor of 0.15-0.2 seems to be an optimal value in these simulations at usual superficial gas velocities. The results of the Figure 2 imply that applying EMMS interphase exchange coefficient with an appropriate scale factor causes a more accurate prediction of the bed expansion ratio in the bubbling fluidized bed.

In a bubbling fluidized bed, the bubble, formed at the distributer, grows in size as they rise through the bed and may become as large as the bed diameter. In this case, the bubble size is physically restricted by the walls of the reactor, and slugging regime occurs. Several researchers have experimentally investigated the mechanisms of slugging flow regime and suggested various empirical formulations to determine slug bubble behavior. Stewart and Davidson [36] gave the minimum slugging velocity (U_{ms}) as:

$$U_{ms} = U_{mf} + 0.07\sqrt{gD} \quad (28)$$

Baeyens and Geldart [37] measured the bed height (H_L) for the onset of slugging flow as follows:

$$H_L = 1.3D^{0.175} \quad (29)$$

According to equation (28), the minimum slugging velocity (U_{ms}) is about 0.185 m/s for the given simulation conditions. The superficial gas velocity is above U_{ms}. According to equation (29) the correlated bed height (H_{ms}) for the onset of the slugs is about 0.8 m, and the bed height used in the simulations is 1m. Therefore, the operating conditions employed in the simulations correspond to the slugging conditions. For slugging fluidized beds, the upward velocity of the slugs has been measured by several investigators, as mentioned in Table 2.

Table 2. Summary of measurements of slug rise velocity in the fluidized beds

Reference	Bed diameter (cm)	Particles	Partide diameter (μm)	Partide density (g/cm^3)	U_g/U_{mf}	Given relation
Lanneau, [38]	7.6	Catalyst	70	2	5-76	$U_S = (U_g - U_{mf}) + 0.41(gD)^{0.5}$
Ormiston *et al.* [39]	2.5; 5.7; 14	Catalyst	41.5		1.03-2.5	$U_S = (0.87 - 9.68)(U_g - U_{mf}) + (0.335 - 0.383)(gD)^{0.5}$
Matsen *et al.* [40]	46	Sand	125			$U_S = (U_g - U_{mf}) + 0.35(gD)^{0.5}$
Kehoe and and Davidson [41]	2.54 5.10 10.2	Quartz Catalyst Sand	68-275 55-62 145	2.55-2.83 1.1 2.65	1.34-135.0 2.1-85.5 2.77-13.0	$U_S = (U_g - U_{mf}) + 0.35(gD)^{0.5}$
Thiel and Potter [42]	5.1 10.2 21.8	FCC+Al Glass Sphe-roid	58.6 74.7	1.73 2.45	4.76-133	$U_S = (U_g - U_{mf}) + 0.35(gD)^{0.5}$

Reference	Bed diameter (cm)	Particles	Partide diameter (μm)	Partide density (g/cm^3)	U_g/U_{mf}	Given relation
Fan *et al.* [43]	10.2 15.3 20.3	Sand	491 711 1122	2.62 2.64 2.65	1.2-3.5	$U_S = 2.43\left(\frac{d_p}{D}\right)^{-0.5}\left(\frac{\rho_s}{1000\rho_g}\right)^{-4.2}(U_g - U_{mf}) + 0.35(gD)^{0.5}$
Satija and Fan [44]	10.2	Glass Beads Alumi-num	1000 2320 5500 6900	2.77 3.537	0.2-1.5 1.4-1.5 0.5-1.5	$U_S = 1.43\left(\frac{d_p}{D}\right)^{-0.9}\left(\frac{\rho_s}{1000\rho_g}\right)^{-4.2}(U_g - U_{mf}) + 0.35(gD)^{0.5}$

In order to validate simulation results, they were compared with the experimental data for three gas flow rates. In addition, these results were compared with predictions of two correlations reported by Fan *et al.* [43] and Satija and Fan [44] relating slug velocity to diameter and density of particles.

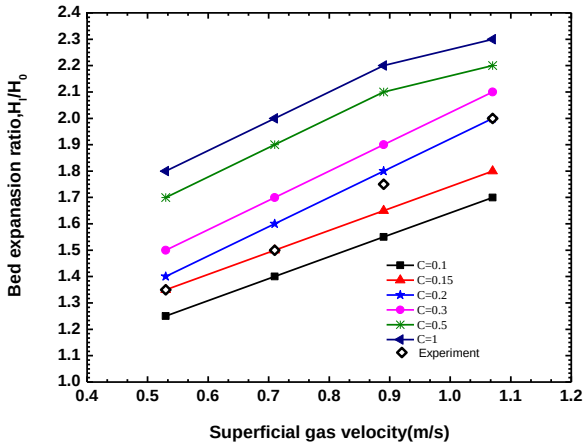

Figure 3. Experimental and predicted slug rise velocity with increasing gas velocity

The simulation results and perditions of the correlations as well as the experimental data are shown in Figure 3. They indicate increasing inlet gas velocity leads to a greater slug velocity. This figure shows the CFD simulation results are in good agreement with the measured data. The figure elucidates that the correlations over predict slug velocity since they do not cover all the range of material properties and operating conditions.

Experimental data show that the bubble size in the fluidized bed grows with gas velocity and with the height above the distributor. At constant velocity, the growth of a bubble is due to three factors [45]:

1. The effective hydrostatic pressure decrease towards the top of the bed.
2. The bubble coalesce in the vertical direction with the trailing bubbles catching up the leading bubble
3. The bubbles coalesce in the horizontal direction with the neighboring bubbles.

The effect of the hydrodynamic pressure is usually small, and the bubble grows in size owing largely to coalescence. Where the bubbles are close enough, coalescence occurs typically when a trailing bubble catches up with a leading bubble [45]. The trailing bubble speeds up as it reaches the wake of the leading bubble and is drawn into the leading bubble [46]. When the bubbles are not in a vertical alignment, the lower bubble first drifts sideways behind the upper bubble and then rises into the upper bubble. A large bubble rising behind several smaller bubbles sweeps them up.

In Figure 4 the simulation results and experimental data of the coalescence of three bubbles are shown. The simulation results very clearly indicate that the trailing bubble catches up with a leading bubble resulting in the coalescence.

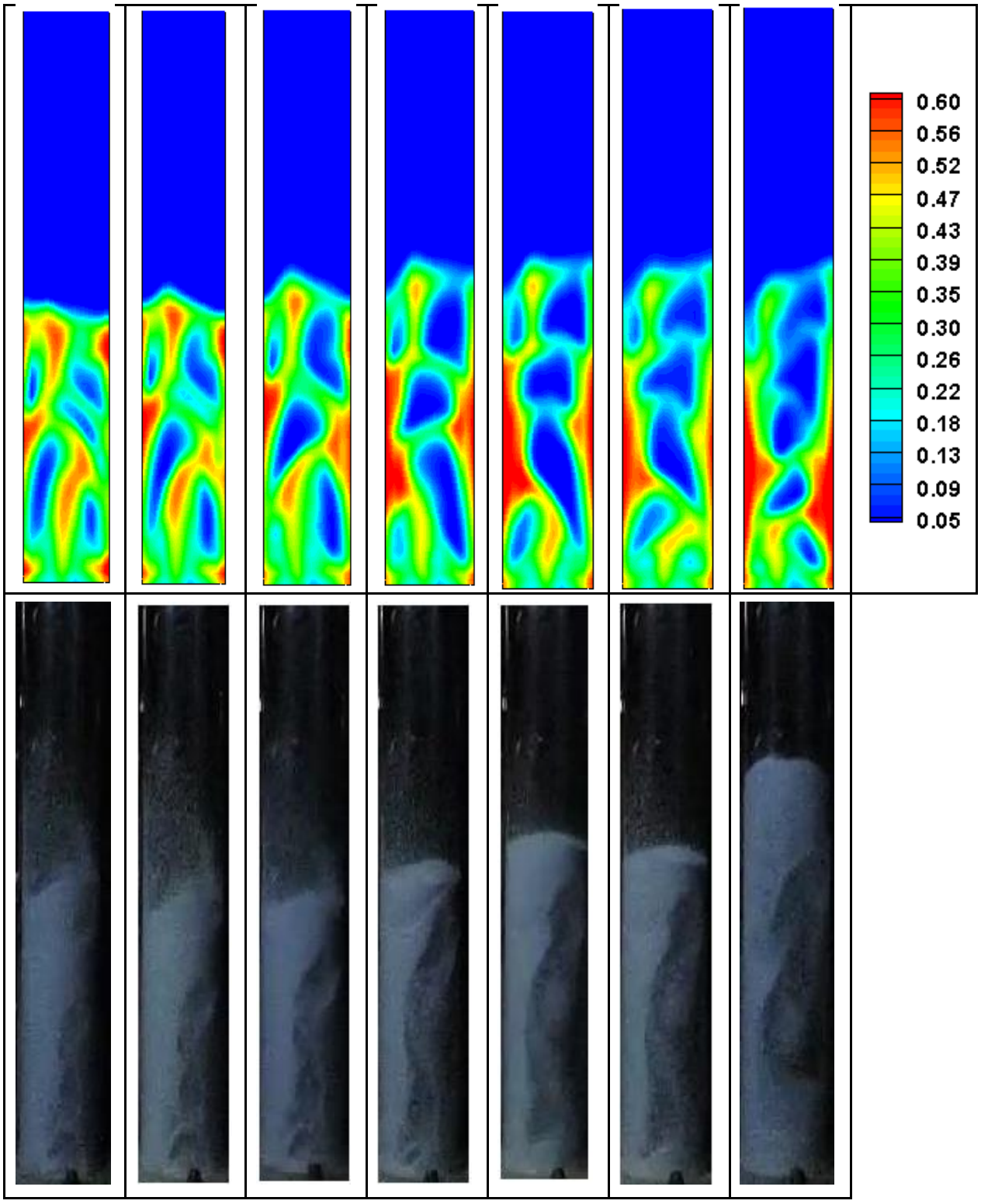

Figure 4 Comparison between simulation (top) and experimental (button) results for bubble coalescence

Figure 5 displays accurate information of bubble dynamics by showing the voidage contours and solid vectors for inlet gas velocity of 0.71 m/s. From the solid velocity vector, it is understood that solid sorbents at the end of the bed move upward at the center of the bed. The coalescences of the bubbles at the bed surface change them to a larger bubble and then it

breaks, causing the solid particles to disperse to the wall. The particles spread on the wall surface above the bed and then fall down near the wall due to the low velocity of the gas phase in the near-wall region. This phenomenon is in accordance with the experimental data reported in the literature [47-48]

Figure 5b shows the flow pattern around and inside the bubble, obtained using Davidson model. According to this model, the pressure at the end of the bubble is lower than the pressures around and at the top of it, and so the fluid is circulated as displayed in Figure 5b. The simulation velocity vectors around a bubble are consistent with those of Davidson model.

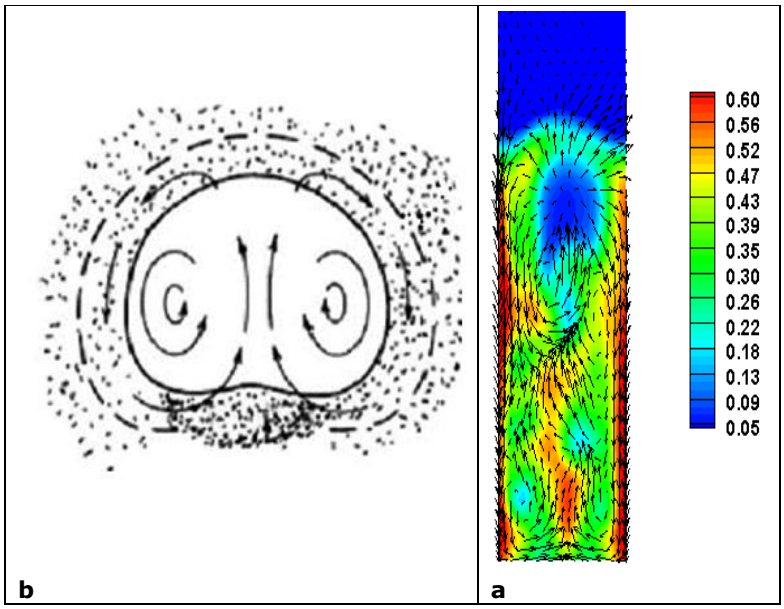

Figure 5. Comparison between simulation results and Davidson model predictions around the bubble a: simulation voidage contours and solid velocity vector, b: flow pattern around the bubble from Davidson model.

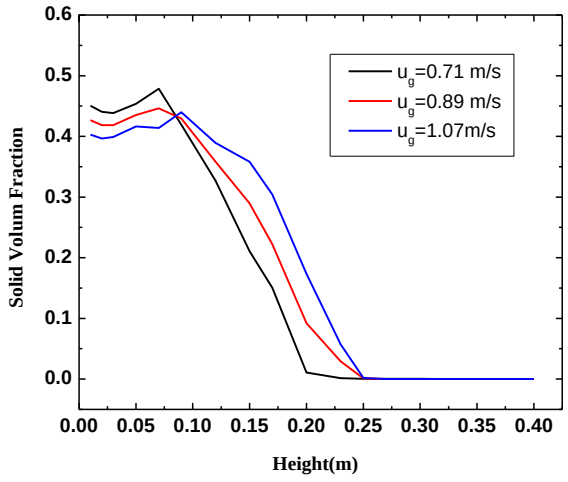

Figure 6. The time-averaged solid volume fraction versus the bed height in different inlet gas velocity

Variation of the inlet gas velocity changes the hydrodynamic and volume fraction distribution of each gas and solid phases [45]. The speed of the adsorption reaction is a function of the solid phase concentrations. In other words, the adsorption rate is higher wherever the volume fraction of the solid phase is larger. A higher input gas velocity causes less density of the solid phase at the entrance of the bed, leading to lower the reaction rate at the bottom of the bed. On the other hand, higher gas velocity increases the height of the bed, causing more contact time of the solid adsorbent with the gas mixture, leading to more adsorption of CO_2. Therefore, two competitive factors affect CO_2 adsorption level when the input velocity of the gas mixture is changed.

In order to investigate the effect of fluidized bed inlet flow rate, the profiles of volume fraction of the solid phase and CO_2 concentration were plotted against the bed height, as shown in Figure 6. As expected, the profiles of volume fraction in Figure 6 show that the density of the solid phase is higher, where gas velocity and bed height are lower.

4.2. Modeling of adsorption process in the fluidized bed reactor

The results of combined hydrodynamic and kinetic models of CO_2 adsorption process in the bubbling gas-solid fluidized bed has been described in this section. A kinetic model, according to equation (24) has been utilized in order to investigate the adsorption of CO_2 by the solid particles (K_2CO_3)). The inlet gas flow velocity to the bed was 0.71 m^3/s, with 15% molar fraction of moisture and carbon dioxide at the reactor inlet. Time-averaged CO_2 concentration profiles at different times are depicted in Figure 7. At the beginning of the bed, variations of carbon dioxide concentration are significant due to the high concentration of CO_2 and H_2O and volume fraction of the adsorbent particles leading to a higher reaction rate of the adsorption. This figure displays the height of the gaseous mixture gradually increases, and CO_2 concentration continuously decreases along the bed. Due to the dependency of the reaction rate to the volume fraction of the solid adsorbent, this trend continues until the adsorption reaction of CO_2 is terminated owing to the low volume fraction of the adsorbent particles. According to Figure 4, the volume fraction of the adsorbent in some areas such as near the walls is high, so dependency of the reaction rate to adsorbent volume fraction leads to high reaction rate causing the concentration of CO_2 to be low near the walls.

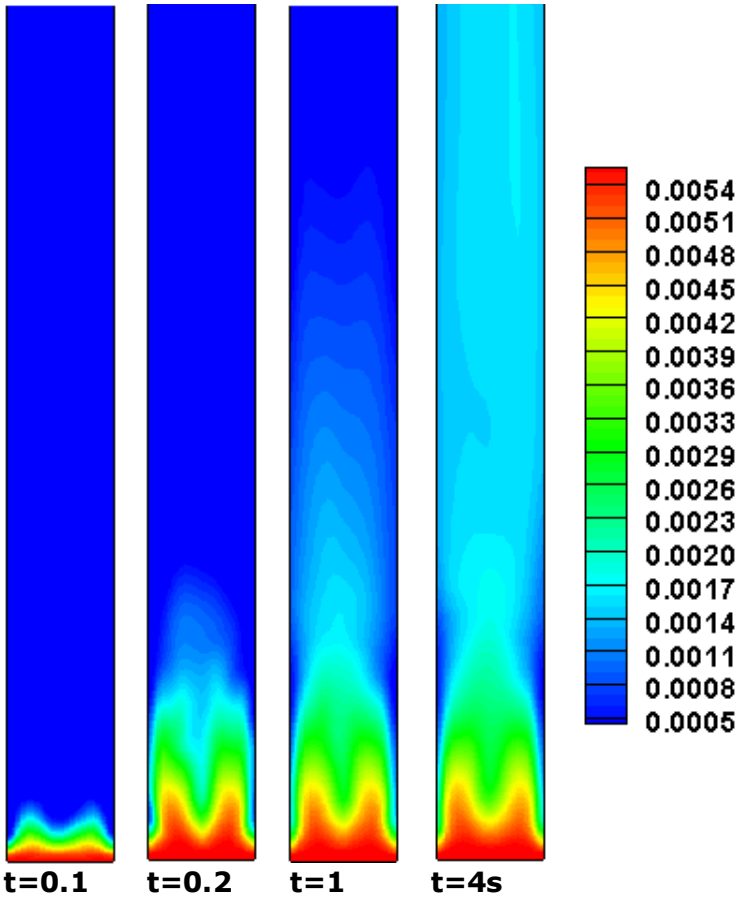

Figure 7. Time-averaged CO_2 concentration (kg/m^3) in different time (ug =0.71 m/s and 15% inlet mole fraction of CO_2 and H_2O)

Area-averaged in different height and time-averaged concentration profile and CO_2 removal content from gas flow in the fluidized bed reactor versus bed height are illustrated in Figure 8. Concentration and removal extent of CO_2 at the top of the reactor are 0.0016 $kmol/m^3$ and 72.4%, respectively. This removal extent using adsorption process by solid particles is comparable with the industrial scale amine or mono-ethanolamine scrubbing method, which is

reported to be 70%. Therefore, it can even be expected that higher adsorption contents of CO_2 can be achieved through optimization of the operational conditions.

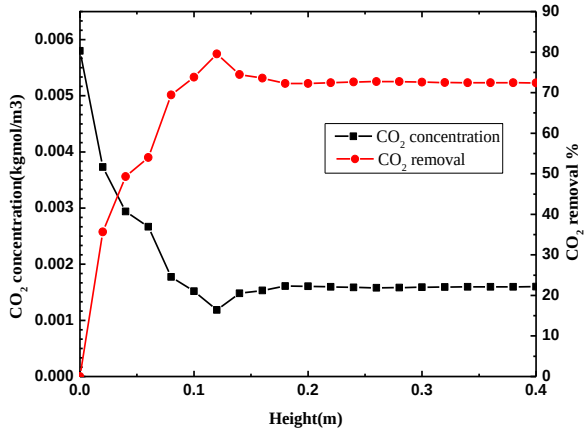

Figure 8. Time and area-averaged CO_2 mass fractions and percent removal of CO_2 versus the reactor height (u_g =0.71 m/s and 15% mole fraction of CO_2 and H_2O)

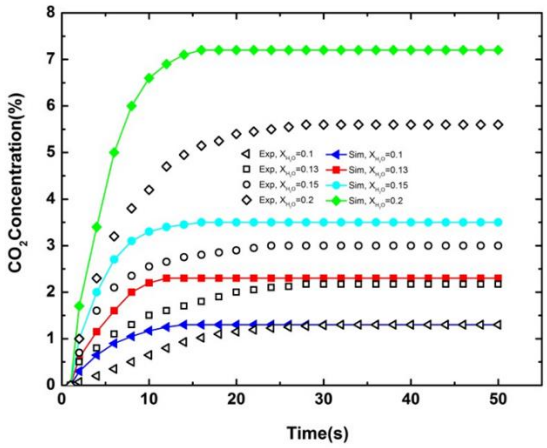

Figure 9. Comparison of the calculated bed outlet CO_2 concentration with the experimental data in different inlet CO_2 concentration

4.2.1. The effect of inlet CO_2 and H_2O concentrations on carbonization reaction

In this section, the effects of the inlet carbon dioxide and water vapor content on the outlet CO_2 concentration were examined. To investigate the effect of the CO_2 concentration, CFD simulations have been implemented under constant baseline operating conditions and different inlet mole fractions of CO_2 (10, 13, 15, 20) and the foregoing results have evaluated with corresponding experimental data. As indicated in the Figure 9, the outlet CO_2 increases with the increase of inlet CO_2 concentrations. The carbonation reaction rate in the high concentration of inlet CO_2 increases, but due to the short of gas resistance time and relatively low H_2O concentration especially in 20%, by increasing inlet CO_2 concentration, the outlet CO_2 increases according to both simulation results and experimental measurements. The simulation results of the CO_2 concentrations at the reactor outlet well agree with experimental data except for 20% inlet concentration, which is much higher, due to the lateral reaction of CO_2 adsorption occurred in high CO2 concentration. The similar pattern of the lateral reaction of CO_2 adsorption was described by Zhao *et el.* [13].

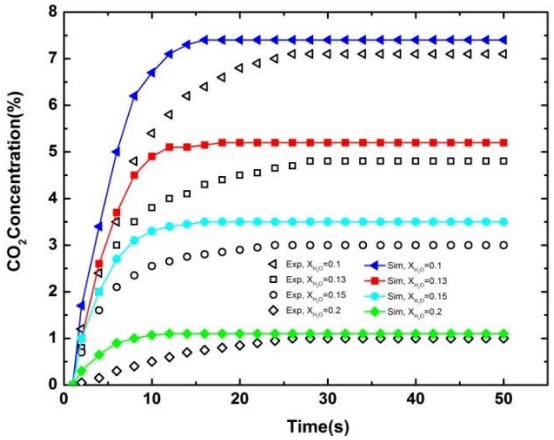

Figure 10. Comparison of the calculated CO_2 removal by CFD model and experimental data different inlet H_2O concentration

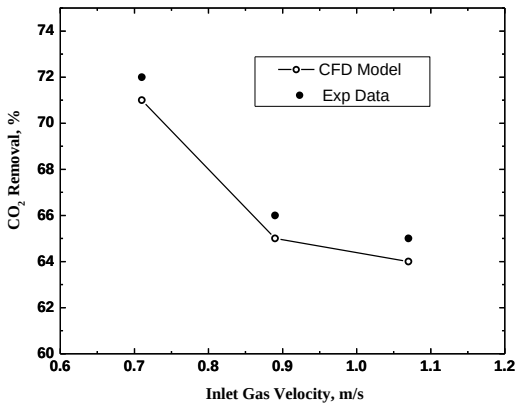

Figure 11. Comparison of the calculated CO2 removal with experimental data in different inlet gas velocity

The effect of the water vapor content in the fluidized bed inlet gas on the CO_2 removal obtained from the experiment and simulation results was shown in Figure 10. The experimental results show that outlet CO_2 concentration decreases from 7.2 to 1.1%, and CO_2 removal increases from 52 to 90% when H_2O concentration in the gas mixture is ranging from 10 to 20%. As H_2O concentration increases, the higher content of H_2O diffuses on the surface of the sorbent, and the adsorption capacity of CO_2 is improved. Therefore, the reaction rate and CO_2 adsorption increase as H_2O concentration increases. A comparison between the predictions of the CFD model with the experimental results shows that the effect of H_2O concentration on CO_2 capture is relatively well estimated by the model. The maximum error of about 14% is found.

4.2.2. The effect of inlet flow rate

The effect of inlet gas mixture flow rate on the CO_2 removal was performed in operational conditions of 15% H_2O and 15% CO_2. Figure 11 shows the results of the CFD simulation and laboratory analysis for 0.71, 0.89, and 1.1m/s gas velocities. The experimental results show that CO_2 removal reaches to 72% at the lowest velocity (0.71 m/s) and 65% at the velocity of 1.1 m/s. The results indicate little change in the amount of CO_2 elimination due to the velocity variation from 0.89 to 1.1 m/s.

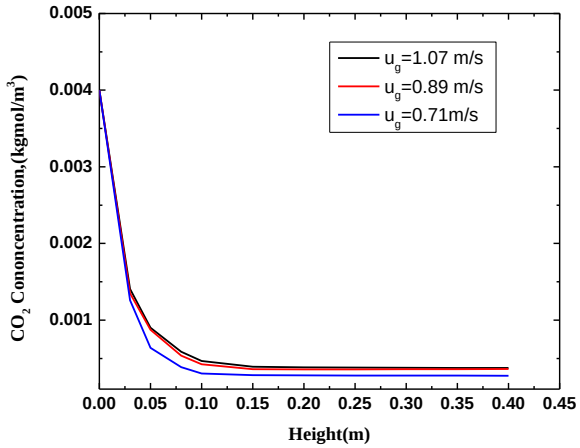

Figure 12. The output CO_2 concentration versus the bed height in the different inlet gas

Figure 12 shows the changes in CO_2 concentration versus the bed height at three different gas velocities. By increasing the height, the amount of available CO_2 in the bed is decreased due to adsorption reaction and lower volume fraction of the solid phase. Consequently, the rate of reaction is decreased so that CO_2 concentration ultimately reaches a constant value where there is no solid. For gas velocity of 0.71 m/s, due to the high density of solid phase at the bottom of the bed, CO_2 concentration has drastically dropped so at the lower height (0.1 m) it has reached to 0.000274 kgmol/m^3. With increasing superficial gas velocity to 0.89 m/s, changes of CO_2 concentration continue up to 0.15 m of height where it reaches to 0.00036 kgmol/m^3. Then at this velocity,output concentration at this height is relatively larger compared to that of the velocity of 0.71 m/s. By setting the input speed at 1.1 m/s, CO_2 concentration reaches to 0.00037 kgmol/m^3 at 0.25m height, which reveals that the height of CO_2 concentration variations is up compared to that of the previous velocity. However, there are small changes in the amount of adsorption. This means that increasing in the adsorption due to increasing the contact time of the gas solid, compensates the effect of the reaction deceleration.

5. Conclusion

In this research, CO_2 adsorption from a flue gas stream using potassium carbonate particles was investigated employing both experimental work and CFD techniques in a bubbling gas solid fluidized bed. The kinetic theory of granular flow was applied in the CFD model to simulate CO_2 capture process, including hydrodynamic characteristics of the bed and adsorption chemical reactions. A modified EMMS interphase exchange coefficient was used, employing a scaling factor, to reduce the universal drag laws, which accounts for the effect of particle clustering. Computational model and experimental measurements elucidate that the bed expansion is increased at higher superficial velocities of the gas due to the larger repulsive forces applied on the particles.

Qualitative analysis of the CFD simulation and experimental results for the bubble behavior revealed that the bubble size in the fluidized bed grows with the heights of the bed above the distributor, owing largely to the coalescence of the bubbles. The computational model results of the slug rise velocity have been compared with the experimental data and predictions of two correlations in different gas flow rates. The CFD results are in good agreement with the measured experimental data, although the correlations overpredict the slug velocity. Other quantitative simulation results indicate that the solid velocity vectors with voidage contours and also solid phase flow pattern around the bubble are similar to those of the well-known Davidson model. In addition, perditions of formation of a dense product layer over the solid reactants and a decline in the rate of the reactions are in good agreement with the experimental data. The effects of different reaction conditions (e.g., gas velocity (1.7–3.0 m/s), CO_2 and H_2O concentrations (7–30%)) on CO_2 adsorption were examined both computationally and experimentally. The experimental results show that increasing the water vapor content and decreasing the gas velocity leads to the increase of CO_2 removal rate. To achieve high CO_2 removal, H_2O concentration must be maintained at a high value. The obtained results indicate that H_2O concentration is the key factor, and it is important to control it. The calculated exit CO_2 concentrations are in relatively good agreement with the experiment data.

References

[1] Seo Y, Jo SH, Ryu HJ, Bae DH, Ryu CK, Yi CK. Korean J. Chem. Eng., 2007; 24: 457.
[2] Solomon S, Qin D, Manning M, Chen Z, Marquis M, Averyt KB, Tignor M, Miller HL. IPCC AR4 WG1, Cambridge, Cambridge University Press, 2007.
[3] Metz B, Davidson O, Coninck HD, Loos M, Meyer L. IPCC special report on carbon dioxide capture and storage, New York, Cambridge University Press, 2005.
[4] Pennline HW, Luebke DR, Jones KL, Myers CR, Morsi BI, Heintz YJ, Ilconich JB. Fuel Process. Technol., 2008; 89: 897.
[5] Duke M, Ladewig B, Smart S, Rudolph V, Diniz da Costa JC. Front. Chem. Sci. Eng., 2010; 4: 184.
[6] Karadas F, Atilhan M, Aparicio S. Energy & Fuels, 2010; 24: 5817.
[7] Yang H, Xu Z, Fan M, Gupta R, Slimane RB, Bland AE, Wright I. J. Environ. Sci., 2008; 20: 14-27.
[8] Dutcher B, Fan M, Leonard B. Sep. Purif. Technol., 2011; 80: 364
[9] Kianpour M, Sobati MA, Shahhosseini S. Chem. Eng. Res. Des., 2012; 90(11): 2041-2050
[10] Hayashi H, Taniuchi J, Furuyashiki N, Sugiyama S, Hirano S, Shigemoto N, Nonaka T. Ind. Eng. Chem. Res., 1998; 37: 185-191.
[11] Lee SC, Choi BY, Lee TJ, Ryu CK, Ahn YS, Kim JC. Catal. Today; 2006, 111: 385.
[12] Li L, Li Y, Wen X, Wang F, Zhao N, Xiao F, Wei W, Sun Y. Energy & Fuels, 2011; 25: 3835.
[13] Zhao C, Chen X, Zhao C, Liu Y. Energy & Fuels, 2009; 23: 1766.
[14] Zhao C, Chen X, Zhao C. Int. J. Greenhouse Gas Control, 2010; 4: 655.
[15] Zhao C, Chen X, Zhao C. Energy & Fuels, 2012; 26: 1401.
[16] Yi CK, Jo SH, Seo Y, Lee JB, Ryu CK. Int. J. Greenhouse Gas Control, 2007; 1: 1235.
[17] Ranade V. Computational Flow Modeling for Chemical Reactor Engineering, Academic press, London, 2002.
[18] Behjat Y, Shahhosseini S, Hashemabadi SH. Int. Commun. Heat Mass Transfer, 2008; 35: 357.
[19] Khongprom P, Gidaspow D. Particuology, 2010; 8: 531.
[20] Garg R, Shahnam M, Huckaby ED. 7th International Conference on Multiphase Flow, ICMF 2010, Tampa, FL, May 30 – June 4, 2010.
[21] Chalermsinsuwan B, Piumsomboon P, Gidaspow D. AICHE J., 2010; 56: 2805.
[22] Syamlal M, Rogers W, O'Brien TJ. MFIX Documentation: Theory Guide, U.S. Department of Energy, Office of Fossil Energy, Morgantown, Virginia, 1993.
[23] Wachem BGMV, Schouten JC, van den Bleek CM, Krishna R, Sinclair JL. AICHE J., 2001; 47: 1292-1302.
[24] McKeen T, Pugsley T. Powder Technol., 2003; 129: 139.
[25] Taghipour F, Ellis N, Wong C. Chem. Eng. Sci., 2005; 60: 6857.
[26] Arastoopour H, Gidaspow D. Powder Technol., 1979; 22: 77.
[27] Seu-Kim H, Arastoopour H. Can. J. Chem. Eng., 1995; 73: 603.
[28] Wang J, van den Hoef MA, Kuipers JAM. Chem. Eng. Sci., 2009; 64: 622.

[29] Yang N, Wang W, Ge W, Li J. Chem. Eng. J., 2003; 96: 71.
[30] Sharonov VE, Okunev AG, Aristov YI. React. Kinet. Catal. Lett. 2004; 82: 363.
[31] Park SW, Sung DH, Choi BS, Lee JW, Kumazawa HJ. Ind. Eng. Chem., 2006; 12: 522.
[32] Wang X, Jin B, Zhong W, Xiao R. Energy & Fuels, 2010; 24: 1242.
[33] Ayobi M, Shahhosseini S, Behjat Y. J. Taiwan Inst. Chem. Eng., 2014; 45(2): 421.
[34] Grace JR, Sun G. Can. J. Chem. Eng., 1991; 69: 1126.
[35] Chalermsinsuwan B, Gidaspow D, Piumsomboon P, Chem. Eng. J., 2011; 171: 301.
[36] Stewart PSB, Davidson JF. Powder Technol., 1967; 1: 61.
[37] Baeyens J, Geldart D. Chem. Eng. Sci., 1974; 29: 255.
[38] Lanneau K. Trans. Instn. Chem. Engrs, 1960; 38: 125-143.
[39] Ormiston R, Mitchell F, and Davidson JF. Chemical Engineering Research and Design, 1965; 43: pp. 209-216.
[40] Matsen J, Hovmand S, and Davidson JF. Chemical Engineering Science, 1969; 24(12): 1743-1754.
[41] Kehoe P, and Davidson JF, in Proceeding of Chemeca, Institution of Chemical Engineers Symposium Series. Australia: Butterworths. 1970; 33:97-116.
[42] Thiel W, and Potter OE. Ind.Eng .Chem. Fundam, 1977; 16(2): 242-247.
[43] Fan LT, Ho TC, Walawender WP. AIChE J., 1983; 29(1): 33-39.
[44] Satija S, Fan LS. AIChE J., 1985, 31(9): 1554-1565.
[45] Kunii D, Levenspiel O. Fluidization engineering, Butterworth-Heinemann, Boston, 1991.
[46] Davidson JF, Clift R, Harrison D. Fluidization, Second ed, Academic Press, 1985.
[47] Laverman JA, Roghair I, van Sint Annaland M, Kuipers JAM. Canadian journal of chemical engineering, 2008; 86(3): 523-535.
[48] Lin JS, Chen MM, Chao BT. AIChE Journal, 1985; 31(3): 465–473.

To whom correspondence should be addressed: Dr. Yaghoub Behjat, Process Development and Equipment Technology Division,Research Institute of Petroleum Industry (RIPI), Tehran, Iran E-mail ybehjat@gmail.com